Available online at www.sciencedirect.com
ScienceDirect
Acta Materialia 56 (2008) 2885–2896
Acta MATERIALIA
www.elsevier.com/locate/actamat

Temperature–stress phase diagram of strain glass $Ti_{48.5}Ni_{51.5}$

Y. Wang [a,b,c], X. Ren [a,b,c,*], K. Otsuka [a,b,c], A. Saxena [d]

[a] Multidisciplinary Materials Research Center, Xi'an Jiaotong University, Xi'an 710049, China
[b] Department of Physics, Xi'an Jiaotong University, Xi'an 710049, China
[c] National Institute for Material Science, 1-2-1 Sengen, Tsukuba, Ibaraki 305-0047, Japan
[d] Theoretical Division, Los Alamos National Laboratory, Los Alamos, NM 87545, USA

Received 28 November 2007; received in revised form 12 February 2008; accepted 12 February 2008
Available online 18 April 2008

Abstract

The temperature and stress dependence of the properties of a recently discovered strain glass $Ti_{48.5}Ni_{51.5}$, which is a glass of frozen local lattice strains, was investigated systematically. It was found that the ideal freezing temperature (T_0) of the strain glass decreases with increasing stress. When the stress exceeds a critical value $\sigma_c(T)$, the pseudo-B2 strain glass transforms into B19′ martensite. However, the stress–strain behavior associated with such a stress-induced transition showed a crossover at a crossover temperature T_{CR}, which is ~20 K below T_0. Above T_{CR}, the sample showed superelastic behavior; however, below T_{CR}, the sample demonstrated plastic behavior. More interestingly, the σ_c vs. temperature relation for unfrozen strain glass obeys the Clausius–Clapyeron relationship, whereas that for frozen strain glass disobeys this universal thermodynamic law. A phenomenological explanation is provided for all the phenomena observed, and it is shown that all the anomalous effects come from the broken ergodicity of the glass system and a temperature-dependent relative stability of the martensitic phase. Based on experimental observations, a temperature–stress phase diagram is constructed for this strain glass, which may serve as a guide map for understanding and predicting the properties of strain glass.

Keywords: Ti–Ni; Polycrystals; Dynamic mechanical analysis; Martensites; Point defects

1. Introduction

Glass transition is usually observed in complex systems owing to the existence of randomness, which causes frustration in the system so that long-range ordering becomes inaccessible [1,2]. A glass transition has two essential signatures. The first signature is that glass undergoes a dynamic freezing transition from a dynamically disordered state to a "quenched" or "frozen" disordered state [1,3], in which the ergodicity of the system is broken [4–6]. The second signature is that there is no macroscopic symmetry change during a glass transition; thus, glass has the same average structure as its corresponding high temperature phase, which is very different from a symmetry-breaking transition.

Recently, a new class of glass, "strain glass", was found in a Ni-rich Ti–Ni system [7]. The dynamic freezing transition of strain glass was identified by the frequency dispersion of the AC mechanical anomalies, which obeys a Vogel–Fulcher relation [7]. X-ray diffraction investigation shows that there is no average structure change (or macroscopic symmetry change) during the strain glass transition [8]. The local strain-ordered nano-domains were imaged by high-resolution transmission electron microscopy, appearing to be distributed randomly in a B2-like matrix [7]. A recent study further proved that ergodicity is indeed broken during the strain glass transition [9]. Therefore, it seems that the concept of strain glass is now established on a solid experimental basis.

Strain glass is formed by doping a sufficient concentration of point defects (excess solute atoms or alloying elements) into a normal martensitic alloy. The random point defects locally distort the crystal lattice and generate random local stresses in the system. These random local

* Corresponding author. Address: National Institute for Material Science, 1-2-1 Sengen, Tsukuba, Ibaraki 305-0047, Japan. Tel.: +81 29 859 2731; fax: +81 29 859 2701.
E-mail address: Ren.Xiaobing@nims.go.jp (X. Ren).

1359-6454/$34.00 © 2008 Acta Materialia Inc. Published by Elsevier Ltd. All rights reserved.
doi:10.1016/j.actamat.2008.02.032

stresses dictate the local strain order and hence prohibit the formation of long-range strain ordering, i.e. spontaneous martensitic transition [10–12] becomes inaccessible kinetically, although martensite is thermodynamically favorable. Instead, the system undergoes a freezing transition below its freezing temperature, during which dynamically disordered local strains (unfrozen strain glass) transform into frozen locally ordered strains (frozen strain glass) [7,8]. Recent work [9] further showed that strain glass bears a striking similarity to two other classes of glass—relaxor in ferroelectric systems and cluster spin glass in ferromagnetic systems. Relaxor is formed by doping point defects into a normal ferroelectric system, whereas cluster spin glass is formed by doping point defects into a normal ferromagnetic system. Thus, these three types of glasses are physically parallel, and they are termed "ferroic glasses" [9]. It should be noted that recent computer simulation studies on the effect of random defects on martensitic transition [13] and on ferroelectrics [14,15] have showed the existence of a percolation limit for defect concentration, above which the system becomes non-ergodic [13–15].

Although long-range strain ordering cannot occur spontaneously in a strain glass system, it does not mean that the long-range strain order (i.e. martensitic state) cannot be achieved under any condition. Very recently, it was found that the B19′ martensitic state can be induced from a pseudo-B2 strain glass state (either frozen or unfrozen state) by a sufficiently high stress [8]. More interestingly, this stress-induced strain glass-to-martensite transition (STG-M transition) results in a new shape memory effect and superelasticity [8], which are achieved in a system without a spontaneous martensitic transition.

The above facts demonstrate that the properties of a strain glass system are strongly dependent on both temperature and stress. However, a systematic study of the behavior of strain glass as a function of both temperature and stress is lacking. Such a study will ultimately lead to a temperature–stress phase diagram, which will serve as a guide map to predict the properties of strain glass at any temperature–stress state. Therefore, the present work systematically studies the temperature and stress dependence of the properties of a $Ti_{48.5}Ni_{51.5}$ strain glass, and ultimately establishes the temperature–stress phase diagram of this strain glass. This work reveals a number of new phenomena in strain glass, some of which disobey the established thermodynamic principle. It is shown that, by considering the unique non-ergodicity of the glass system and the thermodynamic stability of its "hidden" martensitic state, all observed phenomena can be explained in a consistent way.

2. Experimental procedure

A commercial Ni-rich Ti–Ni alloy with nominal composition $Ti_{48.5}Ni_{51.5}$ was used in the present study. The samples were mechanically polished, followed by chemical etching to remove the affected surface layer. Then they were annealed at 1237 K for 1 h in evacuated quartz tubes and subsequently quenched into room-temperature water to obtain a homogeneous supersaturated Ni-rich Ti–Ni solid solution.

To construct the temperature–stress phase diagram of this strain glass, three phase boundaries in the strain glass system must be determined. One is the phase boundary between the unfrozen and frozen strain glass state. Another two phase boundaries are: (i) the one between the B19′ martensitic state and the unfrozen strain glass state (martensite/unfrozen strain glass); and (ii) the one between B19′ martensitic state and the frozen strain glass state (martensite/frozen strain glass), respectively. The following two sets of experiments were performed to determine these three phase boundaries.

The first set of experiments was designed to determine the phase boundary between the unfrozen and frozen strain glass state (unfrozen strain glass/frozen strain glass), which is actually the ideal freezing temperature vs. stress curve separating the unfrozen and frozen glass. In this study, the stress dependence of the ideal freezing temperature was determined by investigating the DC bias stress dependence of the "anomaly" temperature in its AC dynamic mechanical properties. DC bias stress was restricted to be below the critical stress (σ_c) for the stress-induced STG-M transition. The dynamic mechanical properties, i.e. AC storage modulus and $\tan\delta$ (internal friction), were measured with a Q800 dynamic mechanical analyzer (DMA) from TA Instruments. The dynamic mechanical measurement under DC bias stress was done with a tensile fiber clamp, which can generate a constant DC bias stress superimposed on an oscillating measuring stress. Nevertheless, the dynamic mechanical measurement with zero DC bias stress cannot be performed with the tensile fiber clamp, because it always requires a DC preload. This measurement was thus done with a single cantilever clamp instead. In both cases, the storage modulus and internal friction were measured as a function of temperature and frequency simultaneously in a continuous-cooling (cooling rate 1 K min^{-1}) multi-frequency (0.2–20 Hz) mode.

The second set of experiments was designed to determine the two phase boundaries at a higher stress level; one is the martensite/unfrozen strain glass boundary and the other is the martensite/frozen strain glass boundary. This was done by measuring the stress–strain curve (to observe the stress-induced STG-M transition) over a wide temperature range, from well above the ideal freezing temperature to well below this temperature. The tensile testing was done using a tensile machine Shimazu AG-20KNIT.

3. Results

3.1. Strain glass at low stress: stress dependence of the freezing temperature of strain glass

At a low stress level, stress does not generate a structural change to a strain glass, but it may change the glass transition temperature. The following shows the stress

dependence of the strain glass transition temperature by measuring the DC bias stress dependence of the "anomaly" temperature in its dynamic mechanical properties. From this dependence, the ideal freezing temperature $T_0(\sigma)$ vs. stress (σ) relation can be determined, which is the phase boundary in the phase diagram between the unfrozen and frozen strain glass.

Fig. 1 shows the dynamic mechanical behavior of the $Ti_{48.5}Ni_{51.5}$ strain glass at zero bias stress, $\sigma = 0$. This strain glass exhibits a frequency (ω) dependent dip in storage modulus and a peak in the corresponding internal friction during the strain glass transition, which is similar to previous observations [7,8]. The dip temperature $T_g(\omega)$ of the storage modulus increases with increasing frequency ω, following the Vogel–Fulcher relation $\omega = \omega_0 \exp[-E_a/k_B(T_g(\omega) - T_0)]$, as shown in the inset in Fig. 1. The ideal freezing temperature $T_0(\sigma)$ at $\sigma = 0$ (i.e. $T_0(0)$) is determined to be 163.2 K.

Fig. 2 shows the dependence of the dip temperature of the AC storage modulus on DC bias stress ($\sigma = 0$–148 MPa) at frequency of (a) 20 Hz, (b) 1 Hz and (c) 0.2 Hz, respectively. Here, the stress level is below the critical stress (generally >250 MPa) for inducing a STG-M transition. From Fig. 2, it is found that increasing the DC bias stress from 0 to 148 MPa slightly lowers the dip temperature $T_g(\omega)$, and the effect becomes larger at lower frequencies (by comparing Fig. 2a–c). By fitting the ω–$T_g(\omega)$ curve at different DC bias stress with the Vogel–Fulcher relation, the stress dependence of the ideal freezing temperature $T_0(\sigma)$ is obtained, which is shown in Fig. 2d. The ideal freezing temperature $T_0(\sigma)$ shows a slight decrease with the increase in DC bias stress σ. Interestingly, a similar phenomenon was found in spin glass [16], dipolar

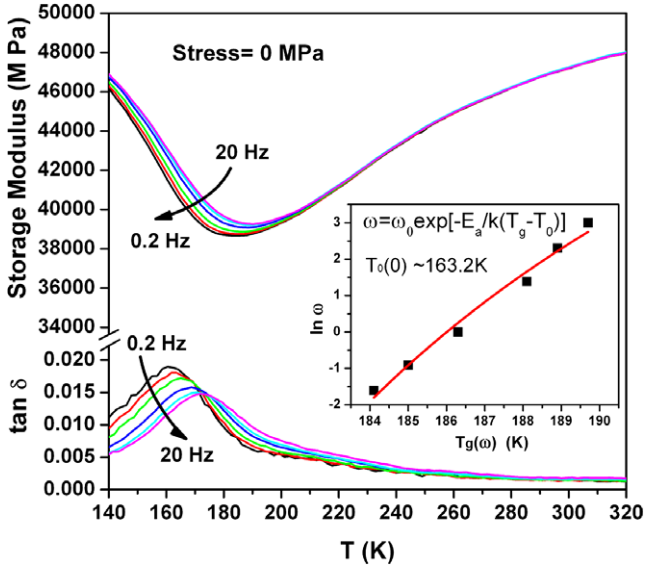

Fig. 1. Frequency dispersion in storage modulus dips and internal friction peaks of a $Ti_{48.5}Ni_{51.5}$ strain glass at zero bias stress. The inset shows the ideal freezing temperature at zero stress, i.e. $T_0(0)$, can be obtained by fitting the frequency (ω) dependence of the storage modulus dip $T_g(\omega)$ with the Vogel–Fulcher relation $\omega = \omega_0 \exp[-E_a/k_B(T_g(\omega) - T_0)]$.

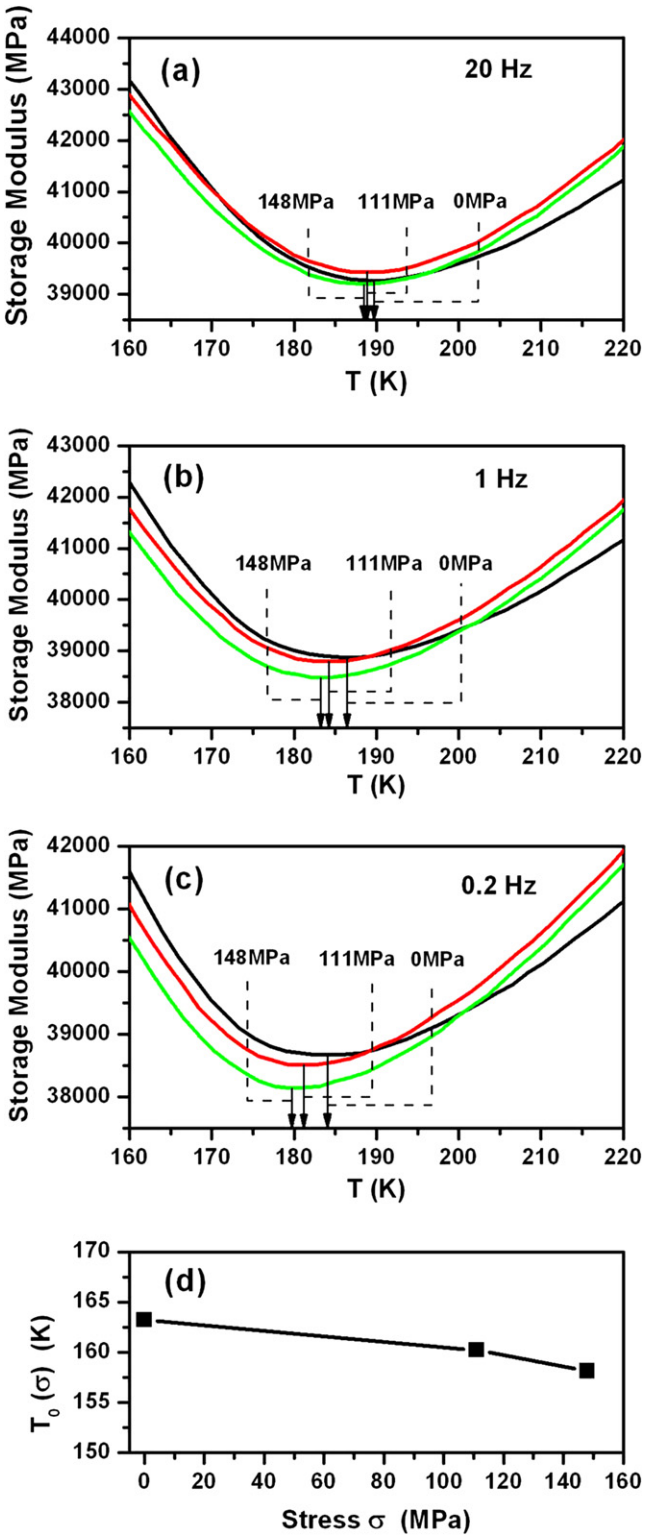

Fig. 2. Dependence of the AC storage modulus and ideal freezing temperature $T_0(\sigma)$ on DC bias stress ($\sigma = 0$–148 MPa) in $Ti_{48.5}Ni_{51.5}$ strain glass: (a), (b) and (c) show the dip temperature (marked by arrow) of AC storage modulus decreases with increasing DC bias stress at frequencies 20 Hz, 1 Hz and 0.2 Hz, respectively; (d) shows that the ideal freezing temperature $T_0(\sigma)$ also decreases with increasing DC bias stress σ.

glass [17] and relaxor ferroelectrics [5], except that the corresponding field is different. Thus, the bias field effect

seems to be a general property for all these ferroic-based glasses.

3.2. Strain glass at high stress: temperature dependence of the deformation behavior and critical stress for stress-induced STG-M transition

At a high stress level, strain glass undergoes a structural change—it transforms into a normal B19′ martensite, as reported in previous work [8]. Here, one is interested in the quantitative change of the deformation behavior of strain glass with temperature, in particular the difference between unfrozen glass ($T > T_0(0)$) and frozen glass ($T < T_0(0)$).

Fig. 3 shows the variation in the deformation behavior of the $Ti_{48.5}Ni_{51.5}$ strain glass with temperature, from well above $T_0(0)$ (unfrozen glass) to well below $T_0(0)$ (frozen glass). It also reveals how the critical stress σ_c for the stress-induced STG-M transition changes with temperature. As depicted in Fig. 3, the $Ti_{48.5}Ni_{51.5}$ strain glass alloy shows a superelastic (recoverable strain) behavior at $T > T_0(0)$. Careful measurements show that the low temperature limit of the superelastic behavior is not exactly at $T_0(0)$, but at a lower temperature T_{CR} (=143 K $\sim T_0(0) - 20$ K), which is the crossover temperature from superelastic behavior to plastic behavior. For $T < T_{CR}$, the alloy shows a plastic (irrecoverable strain) behavior. These results are similar to those reported in previous work [8]. Fig. 3 further shows that, in the superelastic temperature regime ($T > T_{CR}$), the critical stress decreases with lowering temperature; by contrast, in the plastic temperature regime ($T < T_{CR}$), the critical stress increases with lowering temperature. The temperature dependence of the critical stress for the stress-induced STG-M transition forms two phase boundaries, namely martensite/unfrozen strain glass and martensite/frozen strain glass, in the temperature–stress phase diagram.

4. The temperature–stress phase diagram of strain glass

From the experimental results presented in Section 3, the temperature–stress phase diagram of $Ti_{48.5}Ni_{51.5}$ strain glass is constructed and is shown in Fig. 4a. At a stress lower than the critical stress σ_c, the strain glass system undergoes a freezing transition from an unfrozen strain glass to a frozen strain glass at its ideal freezing temperature $T_0(\sigma)$, but the average pseudo-B2 structure remains unchanged. The stress dependence of the ideal freezing temperature $T_0(\sigma)$ is the phase boundary between the unfrozen and frozen strain glass. At a stress higher than critical stress σ_c, the B19′ martensitic phase can be induced from either an unfrozen strain glass or a frozen strain glass. The two σ_c–T curves for these two types of stress-induced STG-M transition represent the two phase boundaries, martensite/unfrozen strain glass and martensite/frozen strain glass, respectively. It is important to note that the

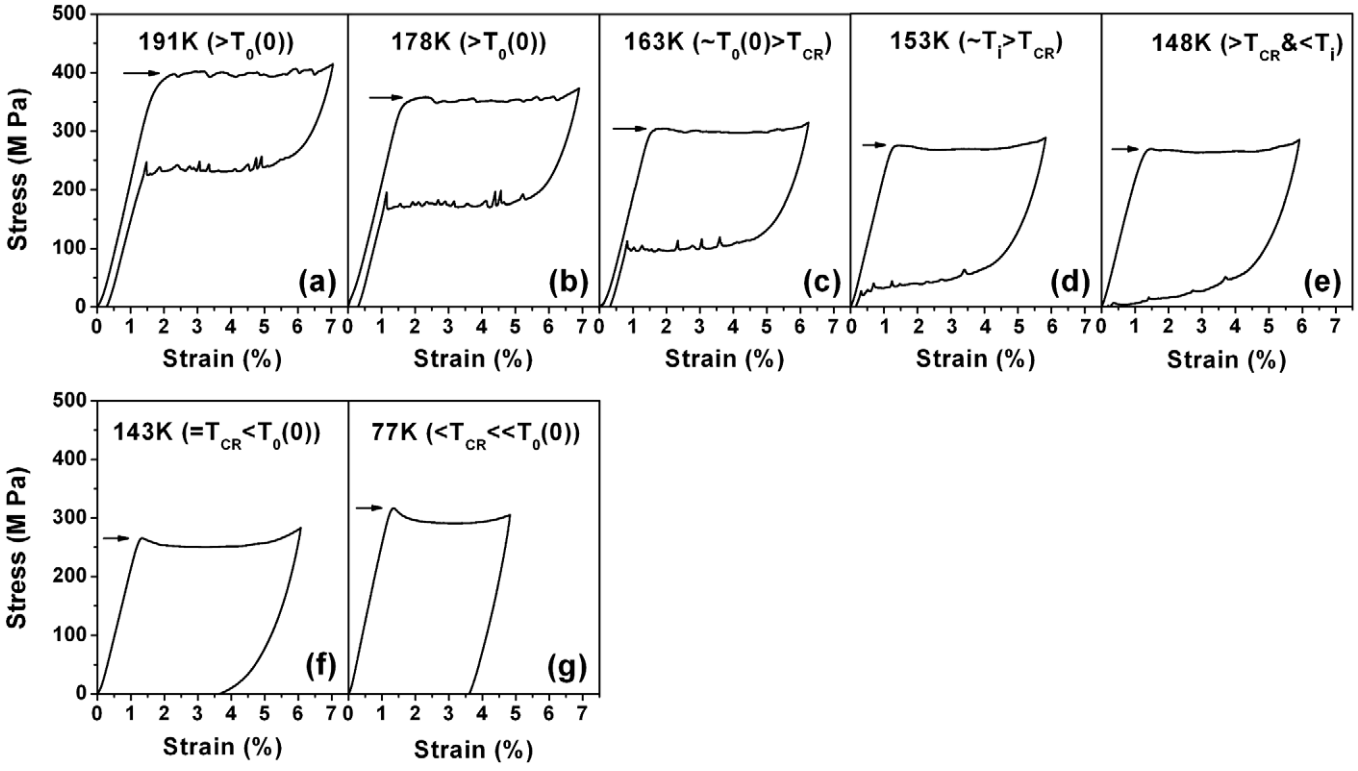

Fig. 3. Deformation behavior over a wide temperature range spanning the ideal freezing temperature at zero stress $T_0(0)$ (=163.2 K) of $Ti_{48.5}Ni_{51.5}$ strain glass. The deformation behavior of strain glass shows a crossover from superelastic behavior to plastic behavior when the system is cooled from a high temperature to a crossover temperature T_{CR}. T_i is the low temperature limit of unfrozen glass under stress.

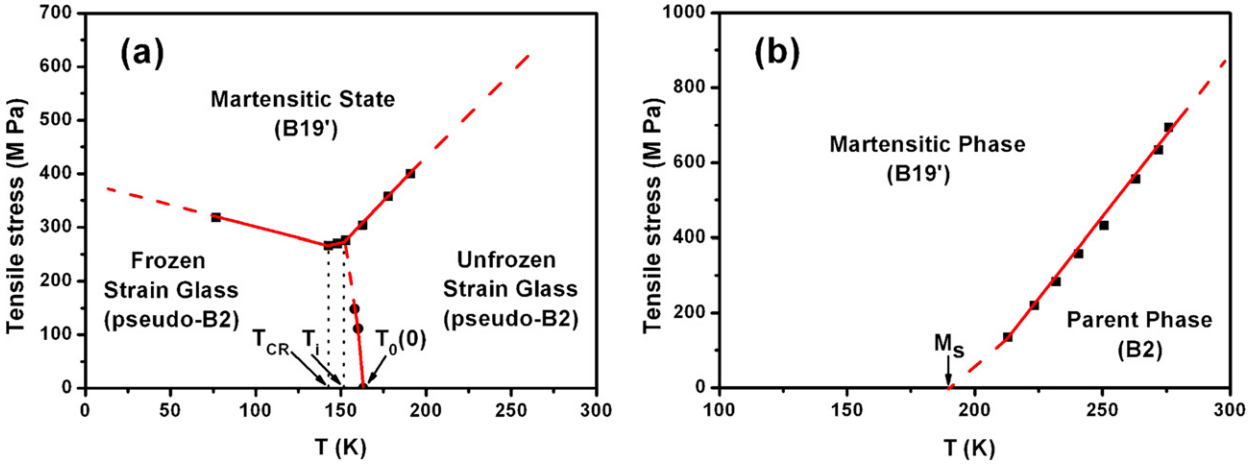

Fig. 4. Comparison between (a) the temperature–stress phase diagram of $Ti_{48.5}Ni_{51.5}$ strain glass alloy and (b) the temperature–stress phase diagram of $Ti_{48.4}Ni_{50.6}$ normal martensitic alloy [16]. $T_0(0)$ in (a) is the ideal freezing temperature at zero stress. T_i in (a) is the temperature of the intersecting point between the unfrozen strain glass/frozen strain glass boundary and the unfrozen strain glass/martensite boundary; it is also the low temperature limit of the unfrozen glass under stress. M_S in (b) is the transition temperature of martensitic transition.

martensite/frozen strain glass boundary is not a phase boundary in the thermodynamic sense. This is because the frozen glass can transform into a martensitic phase above this boundary upon loading, but the martensite formed at high stress cannot go back to the frozen strain glass upon unloading. The reason will become clear in the next section.

Interestingly, the three phase boundaries do not join at one point. The martensite/unfrozen strain glass and martensite/frozen strain glass boundaries intersect at a crossover temperature T_{CR}, which is ~20 K below $T_0(0)$. The strain glass shows superelastic behavior above T_{CR} and plastic behavior below T_{CR}, as shown in Fig. 3. It was also found that the unfrozen strain glass/frozen strain glass boundary intersects the martensite/unfrozen strain glass boundary at a temperature T_i, which is ~10 K above T_{CR} or 10 K below $T_0(0)$. This means that at a stress slightly lower than the intersection stress, during cooling the system first undergoes a glass transition, and then it is followed by a martensitic transition. Such seemingly strange behavior has been experimentally observed and will be reported elsewhere [18].

The three phase boundaries of strain glass shown in Fig. 4a also exhibit interesting features. The unfrozen strain glass/frozen strain glass phase boundary shows that the ideal freezing temperature $T_0(\sigma)$ decreases slightly (~5 K) with increasing DC bias stress up to 148 MPa. This behavior sharply contrasts with the stress effect on a martensitic transition: uniaxial stress (which has a shear component) always increases the transition temperature, as can be deduced from the basic law of thermodynamic phase transitions—the Clausius–Clapyeron relationship. The martensite/unfrozen strain glass boundary shows that the σ_c decreases linearly with decreasing temperature down to T_i (low temperature limit of unfrozen glass under stress), obeying the Clausius–Clapyeron relationship. This is similar to that for a normal stress-induced martensitic transition. In addition, the stress–strain curve of the superelastic behavior (Fig. 3a–c) at $T > T_i$ is also qualitatively the same as a normal stress-induced martensitic transition. However, when in the frozen glass regime ($T < T_i$), the martensite/frozen strain glass boundary shows quite different features from those of martensite/unfrozen strain glass boundary. First, when the system becomes weakly frozen ($T_{CR} < T < T_i$), the slope of the σ_c–T curve becomes smaller compared with that for $T > T_i$, which demonstrates that the stress-induced STG-M transition begins to deviate from the Clausius–Clapyeron relationship. Nevertheless, the stress–strain curve still keeps the superelastic feature in this temperature regime (Fig. 3e). Second, when the system is strongly frozen ($T < T_{CR}$), there is a fundamental change in the σ_c–T relation and the stress–strain behavior. In this temperature regime, σ_c increases with decreasing temperature. This indicates that stress does not favor a phase with high strain, clearly violating the general thermodynamic principle—the Clausius–Clapyeron relationship. Together with this fundamental change in the σ_c–T relation, the stress–strain curve shows plastic behavior (Fig. 3f and g), which is different from that at higher temperatures. These interesting effects are discussed in the next section.

To reveal the difference between a strain glass and a normal martensite, the temperature–stress phase diagram of a normal martensitic system $Ti_{49.4}Ni_{50.6}$ is shown in Fig. 4b for comparison (data are from Ref. [19]). The temperature–stress phase diagram of $Ti_{49.4}Ni_{50.6}$ martensitic alloy shows that a normal martensitic alloy undergoes a spontaneous martensitic transition from B2 parent phase to B19′ martensite at its martensitic transition temperature M_S on cooling. Above M_S, the B2 parent phase can be forced to transform into the B19′martensitic phase by stress. The critical stress for stress-induced martensitic transition

decreases linearly with decreasing temperature, obeying the Clausius–Clapyeron relationship.

Comparing the temperature–stress phase diagram of the strain glass $Ti_{48.5}Ni_{51.5}$ and the normal martensitic $Ti_{49.4}Ni_{50.6}$, one can see that there are only two phases (parent phase and martensite) for a normal martensitic system, but three phases (unfrozen strain glass, frozen strain glass and martensite) for a strain glass system. Obviously, this difference is due to the strain glass transition, during which the system changes from an ergodic state (unfrozen strain glass) to a non-ergodic state (frozen strain glass). The stress-induced STG-M transition in unfrozen strain glass and stress-induced martensitic transition in the parent phase of a normal martensitic system obey the Clausius–Clapyeron relationship; this fact demonstrates that both the unfrozen strain glass and the parent phase of a normal martensitic system are ergodic. However, the stress-induced STG-M transition in frozen strain glass disobeys this general thermodynamic relation; this indicates that the field-induced transition of a non-ergodic glass state cannot be understood within the framework of classical thermodynamics. In the following, a phenomenological free energy landscape for strain glass is proposed, which can provide a comprehensive explanation for all the important physical effects of a strain glass, including the broken ergodicity, the origin of the strain glass transition and stress-induced STG-M transition.

5. Discussion

5.1. Phenomenological free energy landscape for strain glass

Strain glass is formed by doping point defects into a normal martensitic system. Therefore, it is reasonable to consider that a strain glass has a free energy landscape similar to that of a normal martensitic alloy [12,20–22], but with some modifications to allow for the new feature (local ordering) to be described.

In the case of a normal martensitic system, the free energy landscape is usually delineated by a Landau free energy surface in an order-parameter (homogeneous lattice strain) space. The Landau free energy is characterized by the existence of two types of energy valleys, i.e. minima; one is for the parent phase with zero order parameter (or strain), the other represents the martensite with a non-zero order parameter (i.e. a long-range ordering of lattice deformation). A critical temperature T^* exists, at which the free energy of the martensitic valley is equal to that of the parent valley. At $T > T^*$, the martensitic valley is metastable; at $T < T^*$, the martensitic valley is more stable than that of the parent phase.

However, the Landau free energy expresses only homogeneous strain, thus it cannot describe a locally ordered strain system like the strain glass. Therefore, a free energy landscape is needed that can (1) describe the strain instability of the system in the same way as the Landau free energy does, and which has martensite as a candidate phase (so as to be able to explain its possible transition into martensite), (2) describe local strain ordering effect. The free energy landscape (for strain glass) satisfying the above conditions is a three-dimensional (3D) contour shown in Fig. 5a. The free energy is established on a microscopic configuration—average strain space. Each point in the space is a microstate, which represents (1) a microscopic configuration (a particular distribution of nano-domains in the system), and (2) the average strain ε corresponding to this microscopic configuration. It should be noted here that the "configuration coordinate" in Fig. 5a constitutes a thermodynamic phase space (an ensemble of all the microstates with the same average strain). This is analogous to the case of spin glass [1]. The important concept of ergodicity will be discussed later in this phase space.

Fig. 5a shows three important features of the free energy landscape of a strain glass system, as compared with a normal ferroelastic system. First, except for the 3D representation, the free energy F of a strain glass bears much similarity to a standard Landau free energy curve: it also has two types of valley: one for the $\varepsilon = 0$ state (it is shown later that it corresponds to the strain glass), and another for the martensite ($\varepsilon = \varepsilon_M$, where ε_M is the strain of martensite). This can be seen better from a F–ε cross-sectional view of the 3D landscape (Fig. 5b). It will be shown later that the temperature dependence of the martensite valley is also similar to that of a normal martensite system. Secondly, a strain glass can have numerous microstates for the same macroscopic strain, which are depicted as the quasi-degenerate minima in F-configuration cross-sectional view (Fig. 5c, for $\varepsilon = 0$); this is caused by the numerous possible combinations of nano-domains that give rise to the same average strain. Between these different microstates or configurations, random energy barriers exist. Thirdly, the free energy surface is very rough (i.e. high barriers between different microstates) for small average strain ($\varepsilon \to 0$), but it gradually becomes smooth (low barriers) for large average strain (i.e. $\varepsilon \to \varepsilon_M$). This is because a small average strain ($\varepsilon \to 0$) corresponds to a nearly random distribution of the nano-domains, and the change from one microstate to another generally requires the switching/rearrangement of a large number of nano-domains, which corresponds to large barriers. However, for a large average strain ($\varepsilon \to \varepsilon_M$), most of the nano-domains are aligned along the same direction, and thus the change from one microstate to another involves the switching of only a small number of domains; consequently, the barrier is low, and the system can go easily from one state to another. In other words, the system is essentially ergodic as $\varepsilon \to \varepsilon_M$.

To show the 3D free energy landscape in a simpler way, the 3D landscape is projected onto the F–ε plane, and a projected 2D free energy curve is obtained, which is shown in Fig. 5d. The bottom of the free energy curve represents the average strain (ε) dependence of the average free energy (F) of all the microscopic configurations corresponding to a given macroscopic strain state. Note that this free energy curve has a shape similar to the Landau free energy,

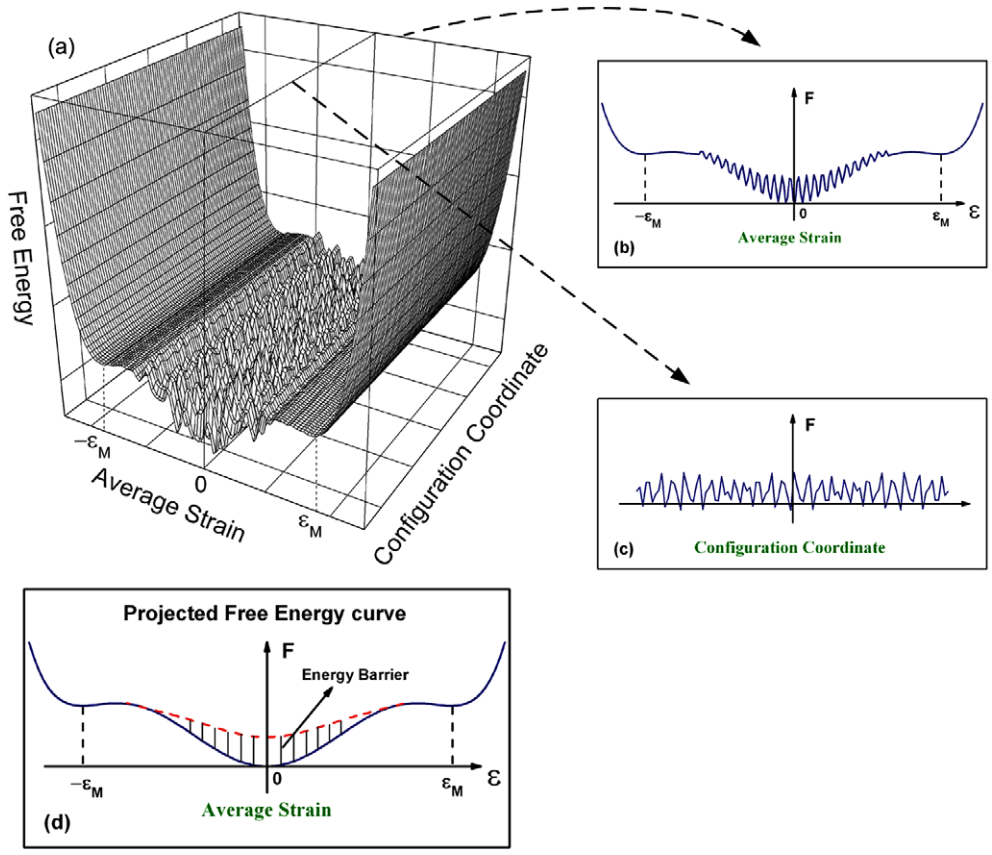

Fig. 5. The free energy landscape of a strain glass in a phase space: (a) 3D free energy landscape of a strain glass in the microscopic configuration coordinate—average strain space; (b) and (c) are two sectional views of the 3D free energy landscape, i.e. free energy vs. average strain (ε), and free energy (F) vs. microscopic configuration at a zero strain, respectively; (d) projected free energy curve in Free energy vs. average strain plane. The solid line is the free energy curve that represents the average free energy as a function of average strain; the difference between the upper dashed curve and the bottom solid curve represents the average energy barrier as a function of average strain.

because the strain glass is derived from a normal martensitic system, and thus it should share a similar free energy curve. However, the projected free energy curve has an important difference from the Landau free energy, that is, it also describes the local barriers between the microscopic configurations. As depicted in Fig. 5d, the difference between the upper dashed curve and the bottom curve represents the average local energy barrier, which decreases gradually with increasing average strain, until it becomes negligible at the martensite state, which is ergodic. It will be seen later that the local barrier of the strain glass is the origin of strain glass formation, and it determines many features of the strain glass.

In the following, the projected free energy curve is used to explain the properties of strain glass and the experimental findings. The temperature dependence of the phase stability of martensite in the projected free energy curve for strain glass is assumed to be qualitatively the same as in the case of standard Landau free energy. As a consequence, the martensitic valley decreases with decreasing temperature in the same way as a normal martensitic system. Therefore, one is able to define a critical temperature T^*, at which $F(\varepsilon_M) = F(0)$, i.e. the free energy of martensite equals that of a zero-strain state. Consequently, martensite is metastable at $T > T^*$ but stable at $T < T^*$. From experimental observation, at $T_0(0)$ the strain glass shows a superelastic/recoverable strain behavior (Fig. 3): one can conclude that martensite is still metastable at $T_0(0)$; thus, an important conclusion, that $T_0(0) > T^*$ for strain glass, is obtained. It is assumed that the local barrier increases with decreasing temperature, and the thermal activation energy k_BT is higher than the local barrier at $T > T_0(0)$ but lower than the local barrier at $T < T_0(0)$, which is similar to the case of spin glass [1]. The above information allows one to define four temperature regimes where strain glass shows different thermodynamic stability, local barriers and thermal activation k_BT. Such differences will give rise to different behavior of the strain glass:

(1) At $T > T_0(0) > T^*$, martensitic state is metastable and $k_BT >$ local barrier, as shown in Fig. 6a.
(2) At $T = T_0(0) > T^*$, martensitic state is still metastable, but $k_BT \approx$ local barrier, as shown in Fig. 6b.
(3) At $T = T^*$, the martensitic state has the same free energy as that of the zero macroscopic strain state, and $k_BT <$ local barrier, as shown in Fig. 6c.

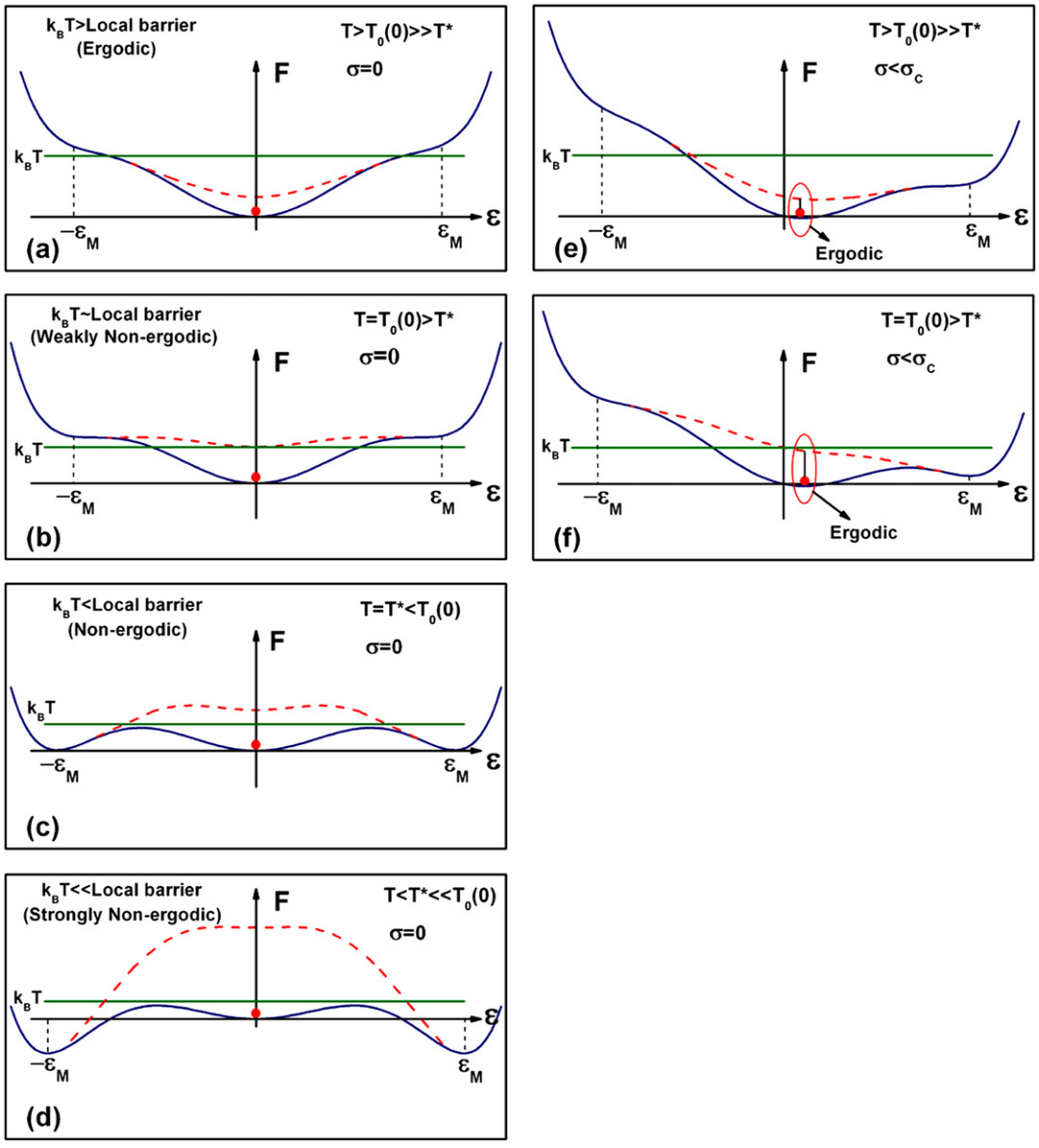

Fig. 6. Phenomenological explanation for the broken ergodicity during the strain glass transition and stress dependence of the ideal freezing temperature of strain glass. F is the free energy; $T_0(0)$ is the ideal freezing temperature at zero stress; T^* is the temperature, at which martensitic state starts to be stable; and σ_c is the critical stress of the stress-induced STG-M transition. (a), (b), (c) and (d) show the projected free energy curve of a strain glass at zero stress for $T > T_0(0) \gg T^*$, $T = T_0(0) > T^*$, $T = T^* < T_0(0)$ and $T < T^* \ll T_0(0)$, respectively; (e) and (f) show the projected free energy curve of strain glass at $\sigma < \sigma_c$ for $T > T_0(0) \gg T^*$, and $T = T_0(0) > T^*$, respectively. The stressed strain glass energetically favors the microscopic configurations with more orderly aligned nano-domains, as circled in (e) and (f).

(4) At $T < T^* < T_0(0)$, the martensitic state is stable and $k_BT \ll$ local barrier, as shown in Fig. 6d.

5.2. Origin of strain glass transition

In the following, the projected free energy curve of strain glass is used to explain why the strain glass system does not undergo a martensitic transition but rather undergoes a glass transition with broken ergodicity.

Fig. 6a shows the projected free energy curve of strain glass at $T > T_0(0) > T^*$. As the free energy of the martensitic state is higher than that of the macroscopic strain states and the thermal activation is much higher than the height of the local barriers, the system takes the zero macroscopic strain state as its stable state. This equilibrium state corresponds to an unfrozen strain glass or an ergodic strain glass, in which the local ordered strains are spatially and dynamically disordered. On cooling, the free energy of the martensitic state decreases continuously, as shown in Fig. 6b–d, and the system has a tendency to transform into martensite at $T < T^*$. However, before reaching the thermodynamic instability temperature T^*, the system becomes frozen into a glassy state at $T_0(0)$ ($>T^*$). This is because,

when the system is cooled to $T_0(0)$, the thermal activation becomes comparable with most of the local barriers (Fig. 6b); thus, it becomes impossible for the system to traverse all the possible microscopic configurations of the zero macroscopic strain state within experimental time. Therefore, the global ergodicity of the system starts to break, i.e. the unfrozen strain glass starts to transform into a frozen strain glass or non-ergodic strain glass at $T_0(0)$. On further cooling to T^*, the martensitic state becomes thermodynamically stable; however, k_BT is lower than the height of the barriers (Fig. 6c), thus the system cannot be activated to the martensitic state and the long-range strain ordering is suppressed. Owing to the limitation of kinetics, the system is trapped into certain configuration of the zero macroscopic strain state and cannot transform into the martensitic state, although the martensitic state becomes more stable at low temperature, as shown in Fig. 6d. This results in a complete breaking of the global ergodicity of strain glass system, and the local ordered strains are completely frozen. Therefore, the strain glass transition and corresponding broken ergodicity originate from the local barrier or kinetic limitation created by the random point defects.

5.3. Decrease in ideal freezing temperature with increasing stress

Now the projected free energy curve of strain glass is used to explain the decrease in $T_0(\sigma)$ with increasing stress σ ($<\sigma_c$), a new effect observed in Fig. 2d. Fig. 6e shows the projected free energy curve of a stressed strain glass at a temperature above $T_0(0)$. It can be seen that the external stress "tilts" the free energy curve, similar to the effect on the Landau free energy of a normal ferroelastic system, as a result of the stress–strain coupling energy $-\sigma\varepsilon$. The physical picture of the tilt in the free energy landscape is that external stress tends to stabilize a macroscopic strain state with a suitable non-zero average strain (as circled in Fig. 6e). Microscopically, the system favors those microscopic configurations, in which nano-domains roughly align along the external stress.

At $T > T_0(0)$, the external stress does not generate a fundamental change in the properties of an unfrozen glass, because the system is ergodic ($k_BT >$ barriers) and the stress does not alter this. At $T = T_0(0)$, the system begins to become non-ergodic ($k_BT \approx$ barrier height) at zero stress (Fig. 6b). In such a case, an external stress can bring about fundamental changes to a frozen glass. When the stressed strain glass is cooled to $T_0(0)$ from a high temperature, the projected free energy curve remains tilted by the external stress during cooling. Thus, the system favors the macroscopic strain state with a non-zero average strain, as circled in Fig. 6f. As discussed above, the local barrier at non-zero macroscopic strain state is lower than that at a zero macroscopic strain state, so the microscopic configurations in the non-zero macroscopic strain state now become ergodic ($k_BT >$ barrier) under stress. In other words, the stressed strain glass actually remains ergodic and does not freeze at $T_0(0)$. In order to freeze the stressed strain glass, further cooling is needed. This explains why the freezing temperature decreases with the application of an external stress. Apparently, the decrease in ideal freezing temperature is more significant with increasing external stress. The decrease in the freezing temperature by stress demonstrates that the external field can delay the onset of non-ergodicity.

The decrease in strain glass transition temperature with increasing external stress is analogous to similar effects observed in many ferroic-based glass systems, such as ferroelectric relaxors [5], spin glass [16] and dipolar glass [17], except for a difference in the nature of the external field (electric field and magnetic field in the latter cases). Therefore, such an effect should be considered a common feature of many glass systems. This feature is very different from the well-known effect of external field on normal ferroic transitions: a unidirectional external field always increases the transition temperature of these transitions, a consequence of the Clausius–Clapyeron law. Clearly, such a difference stems from the non-ergodicity of the glass systems.

5.4. Temperature dependence of the critical stress for stress-induced STG-M transition

The phase diagram of strain glass (Fig. 4a) and the corresponding stress–strain curves (Fig. 3) demonstrates that the strain glass shows different features in the following three temperature regimes: (1) at $T > T_i$ ($>T_{CR}$), the strain glass shows superelastic behavior, and the corresponding stress-induced STG-M transition obeys the Clausius–Clapyeron relationship; (2) at $T_i > T > T_{CR}$, the strain glass also shows superelastic behavior, but the σ_c–T curve for the stress-induced STG-M transition has a smaller slope than case (1); (3) at $T < T_{CR}$, the strain glass shows a plastic behavior and the corresponding stress-induced STG-M transition violates the Clausius–Clapyeron relationship, i.e. the slope of the σ_c–T curve becomes negative. The crossover temperature T_{CR} differentiates plastic behavior at $T < T_{CR}$ and superelastic behavior at $T > T_{CR}$. T_{CR} corresponds to the thermodynamic critical temperature T^*, i.e. $T_{CR} \approx T^*$, which will be discussed later. The following discussion mostly uses T^* rather than T_{CR}, because T^* has a well-defined physical meaning. Next, the free energy landscape of strain glass is used to explain the different behaviors at $T > T_i$ ($>T^*$), $T_i > T > T^*$ ($\sim T_{CR}$) and $T < T^*$ ($\sim T_{CR}$).

At $T > T_i$ ($>T^*$), the strain glass is unfrozen (ergodic) at stress σ_c (Fig. 4a) and exhibits superelastic behavior. The superelasticity of strain glass is attributed to the (unfrozen) strain glass being stable and martensite being metastable in the absence of an external stress (Fig.7a and c). When the system is loaded with a stress exceeding a critical value σ_c, the martensite becomes a stable phase, as shown in Fig. 7b and d; thus, the strain glass transforms into martensite.

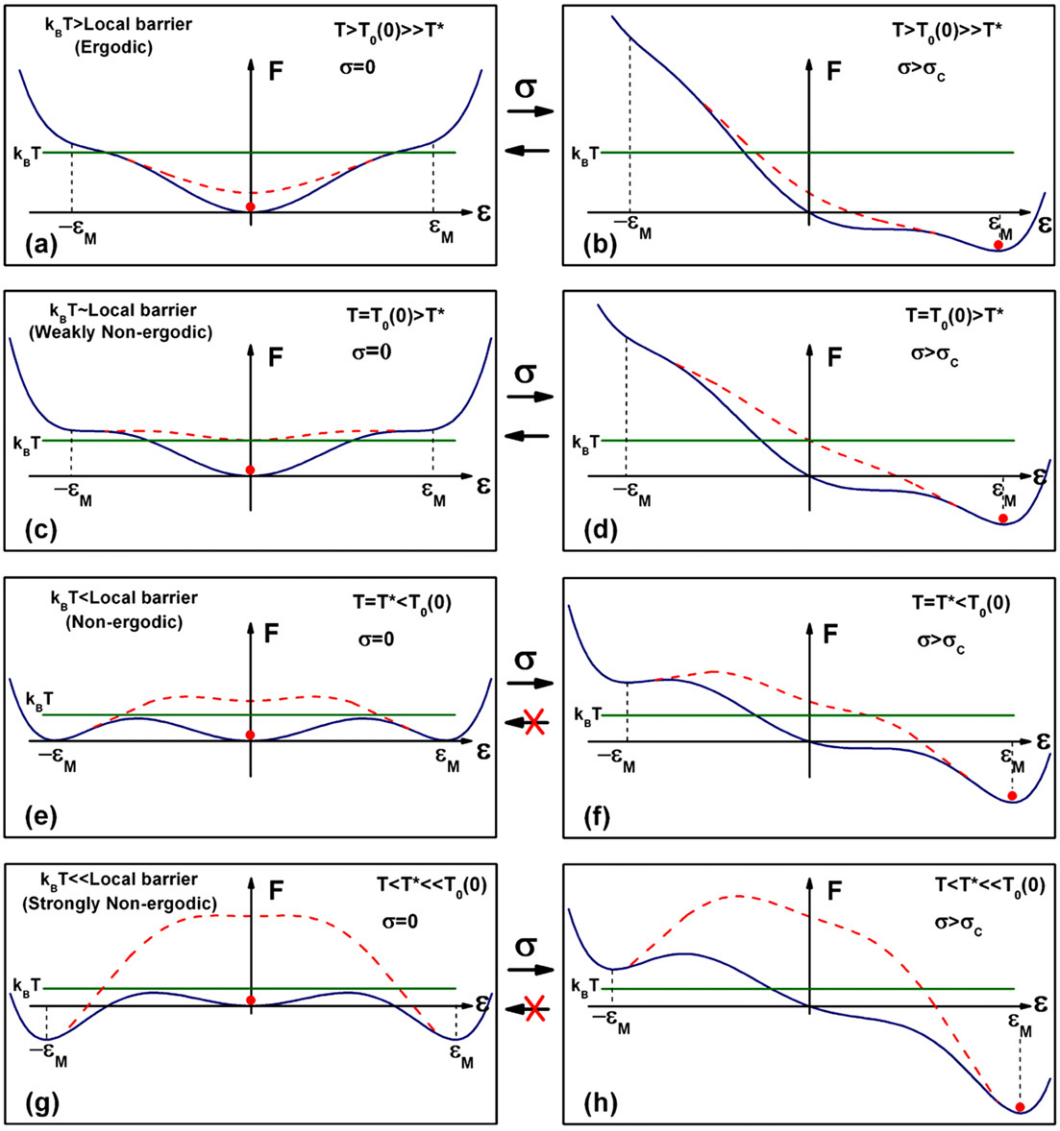

Fig. 7. Phenomenological explanation for the temperature dependence of the deformation behavior of stress-induced STG-M transition. F is the free energy; $T_0(0)$ is the ideal freezing temperature at zero stress; T^* is the temperature at which martensitic state starts to be stable; and σ_c is the critical stress of the stress-induced STG-M transition. (a), (c), (e) and (g) show the projected free energy curve of a strain glass at zero stress for $T > T_0(0) \gg T^*$, $T = T_0(0) > T^*$, $T = T^* < T_0(0)$ and $T < T^* \ll T_0(0)$, respectively; (b), (d), (f) and (h) show the projected free energy curve of strain glass at $\sigma > \sigma_c$ for $T > T_0(0) \gg T^*$, $T = T_0(0) > T^*$, $T = T^* < T_0(0)$ and $T < T^* \ll T_0(0)$, respectively, in which the martensitic state is thermodynamically favorable and dynamically accessible with the assistance of the external stress.

Upon unloading, the induced martensite becomes thermodynamically unstable again, so the system reverts to the original unfrozen strain glass state (Fig.7a and c). This results in the observed superelastic behavior of strain glass. As the free energy difference between the metastable martensite and the strain glass becomes smaller upon cooling, the corresponding σ_c also decreases with decreasing temperature. In addition, at $T > T_i$ ($>T^*$), the strain glass system remains ergodic, so the situation is the same as a normal martensitic system. Thus, the σ_c–T curve is governed by the thermodynamic law—the Clausius–Clapyeron relationship.

At $T_i > T > T^*$ ($\sim T_{CR}$), the strain glass becomes weakly frozen, but it still shows superelastic behavior (Fig. 3e). The reason for the superelastic behavior at $T_i > T > T^*$ ($\sim T_{CR}$) is the same as the case for $T > T_i$: the martensitic state is still metastable, so there is a thermodynamic driving force to revert the stress-induced martensite back to the strain glass. Compared with that for $T > T_i$, the smaller slope of the σ_c–T curve (Fig. 4a) indicates that, besides the above thermodynamic consideration as in the case for $T > T_i$, another important factor – kinetic limitation – is playing a role. At $T_i > T > T^*$ ($\sim T_{CR}$), the thermal activation energy k_BT becomes lower than the local barrier, so an additional external stress is required to assist the system to overcome the local barrier (i.e. kinetic limitation). The additional external stress required makes the slope of σ_c–T curve smaller than without this effect (i.e. at $T > T_i$).

Thus, the change in the slope is a result of the competition between a thermodynamic factor (free energy difference) and a kinetic factor (local barrier). At the temperature range $T_i > T > T^*$ ($\sim T_{CR}$), which is no more than 10 K below T_i, the kinetic limitation is not so strong, as $k_B T$ is just slightly lower than the local barrier. As a result, the behavior of the system is governed mainly by the thermodynamic driving force, which results in superelastic behavior and a decrease in σ_c upon cooling, but with some decrease in the σ_c–T slope due to the kinetic limitation.

At $T = T^*$, the free energy of martensite becomes equal to that of frozen strain glass, but the spontaneous martensitic transition cannot occur owing to the kinetic limitation, as shown in Fig. 7e. When the system is loaded with an external stress σ_c, the local barriers can be overcome, and martensite can be induced, as shown in Fig. 7f. As the martensitic state has the same thermodynamic stability at T^* as the strain glass, it remains even after removing the external stress. Therefore, at $T = T^*$, the strain glass starts to exhibit plastic deformation. Experimentally, one finds that T_{CR} is the crossover temperature from superelastic behavior to plastic behavior, thus $T^* \approx T_{CR}$.

At $T < T^*$ ($\sim T_{CR}$), the strain glass is strongly frozen, and it shows plastic deformation with a negative slope of the σ_c–T line. This is because the free energy of the martensite becomes even lower than that of the frozen strain glass (Fig. 7g), and the induced martensite is energetically stable upon unloading (Fig. 7h). This explains the plastic deformation behavior. The negative slope of the σ_c–T line, i.e. the violation of the Clausius–Clapyeron relationship at $T < T^*$ ($\sim T_{CR}$) is again a result of the competition between the thermodynamic driving force and the kinetic limitation. With temperature decreasing, the thermodynamic driving force towards the martensite becomes larger (as depicted in Fig. 7e and g), and thus this would cause a decrease in σ_c. However, the kinetic limitation (local barrier) of frozen strain glass increases more dramatically (Fig. 7e and g), which leads to a bigger increase in σ_c. As a result, σ_c increases rather than decreases with lowering temperature, violating the Clausius–Clapyeron relationship.

From the above discussion, one can see that both the slope change and the violation of the Clausius–Clapyeron relationship in the frozen strain glass are due to the limitation of kinetics or the broken ergodicity. This also further proves that the strain glass transition is a kinetics-governed freezing transition rather than a thermodynamic phase transition.

6. Conclusion

The stress and temperature dependence of the properties of strain glass was systematically studied. This led to the construction of a temperature–stress phase diagram of a $Ti_{48.5}Ni_{51.5}$ strain glass, which may provide a guide map for understanding and predicting the properties of strain glasses. The following conclusions were obtained:

(1) The ideal freezing temperature of strain glass decreases with the increase in external stress. This demonstrates that an external field can delay the onset of non-ergodicity during a glass transition.
(2) The strain glass undergoes a stress-induced STG-M transition when the external stress is beyond a critical stress σ_c. The deformation behavior of the stress-induced STG-M transition shows a crossover from superelastic behavior to plastic behavior at a crossover temperature T_{CR}.
(3) Strain glass obeys the Clausius–Clapyeron relationship in its unfrozen (ergodic) state; however, in its frozen (non-ergodic) state, it shows a decrease in the slope of the σ_c–T line, and a complete violation of such a universal relation. The slope change and violation of the Clausius–Clapyeron relationship is due to the broken ergodicity of strain glass in the frozen state, and the increase in the relative stability of martensite at low temperature. It further demonstrates that the strain glass undergoes a kinetics-governed freezing transition rather than a thermodynamic phase transition.
(4) With a free energy landscape for the strain glass, which is a Landau free energy established in the configuration-strain space, all the observed effects are found to have a consistent explanation.

Acknowledgements

The present work was supported by Grant-in-Aid for Scientific Research (B) of JSPS, National Science Foundation of China and National Basic Research Program of China under Grant No. 2004CB619303 as well as 111 project of China. The authors thank T. Suzuki, S. Sarkar, X.D. Ding, G.L. Fan, J. Zhang and Y.M. Zhou, for technical support and helpful discussions.

References

[1] Mydosh JA. Spin glasses. Philadelphia: Taylor & Francis; 1993.
[2] Binder K. Glassy materials and disordered solids. London: World Scientific; 2005.
[3] Fischer KH, Hertz JA. Spin glasses. Cambridge: Cambridge University Press; 1991.
[4] Nagata S, Keesom PH, Harrison HR. Phys Rev B 1979;19:1633.
[5] Viehland D, Li JF, Jang SJ, Cross LE, Wuttig M. Phys Rev B 1992;46:8013.
[6] Hessinger J, Knorr K. Phys Rev Lett 1990;65:2674.
[7] Sarkar S, Ren X, Otsuka K. Phys Rev Lett 2005;95:205702.
[8] Wang Y, Ren X, Otsuka K. Phys Rev Lett 2006;97:225703.
[9] Wang Y, Ren X, Otsuka K, Saxena A. Phys Rev B 2007;76:132201.
[10] Otsuka K, Ren X. Prog Mater Sci 2005;50:511.
[11] Khachaturyan AG. Theory of structural transformation in solids. New York: Wiley; 1983.
[12] Salje EKH. Phase transformation in ferroelastic and Co-elastic crystals. Cambridge: Cambridge University Press; 1993.
[13] Semenovskaya S, Khachaturyan AG. Acta Mater 1997;45:4367.
[14] Semenovskaya S, Khachaturyan AG. Ferroelectrics 1998;206–207:157.

[15] Semenovskaya S, Khachaturyan AG. J Appl Phys 1998;83:5125.
[16] Chamberlin RV, Hardiman M, Turkevich LA, Orbach R. Phys Rev B 1982;25:6720.
[17] Höchli UT, Kofel P, Maglione M. Phys Rev B 1985;32:4546.
[18] Wang Y, Ren X, Otsuka K. To be published.
[19] Miyazaki S, Otsuka K, Suzuki Y. Scripta Mater 1981;15:287.
[20] Falk F. Acta Metall 1980;28:1773.
[21] Barsch GR, Krumhansl JA. Phys Rev Lett 1984;53:1069.
[22] Ahluwalia R, Lookman T, Saxena A, Albers RC. Acta Mater 2004;52:209.